Direct detections of the axionlike particle revisited

Wei Chao,[*] Jing-Jing Feng,[†] and Mingjie Jin[‡]
Center for Advanced Quantum Studies, Department of Physics, Beijing Normal University, Beijing 100875, China

(Received 20 November 2023; accepted 4 March 2024; published 29 April 2024)

Axionlike particles (ALPs) are promising dark matter candidates. Their signals in direct detection experiments arise from the well-known inverse Primakoff effect or the inverse Compton scattering of ALPs with the electron. In this paper, we revisit the direct detection of ALP by carefully considering the interference between the inverse Primakoff amplitude and the inverse Compton amplitude in the scattering process $a + e \to e + \gamma$ for the first time. It shows that the contribution of the interference term turns to be dominated in the scattering for a large ALP energy. Given the new analytical formula, signals or constraints of ALP couplings in various projected experiments are investigated. Our results show that these experiments may put strong constraints on ALP couplings for relatively heavy ALP. We further study projected constraints on ALP from the JUNO experiment, which shows competitive constraints on ALP couplings using a ten-year exposure.

DOI: 10.1103/PhysRevD.109.075044

I. INTRODUCTION

The strong *CP* problem finds a solution via the Peccei-Quinn mechanism [1,2], which gives rise to a fascinating prediction; the existence of a new particle called the axion, as outlined in Refs. [3–5]. These ultralight, weakly interacting particles, such as axions or axionlike particles (ALPs), have also gained prominence as potential dark matter (DM) candidates within the diverse theories of DM [6–12]. Since they can couple to the Standard Model (SM) particles such as photon and electron, extensive experimental works [13–16] have been devoted to searching for such particles through the axion-photon coupling or the axion-electron coupling, and stringent limits on these couplings have already been imposed.

The Sun is an excellent source of axions, offering an easily obtainable flux of axions generated in the center of the Sun via various processes [17,18]. However, the endeavor to detect axions or ALPs is an arduous undertaking, primarily due to their extremely weak interactions with SM particles. Fortunately, Sikivie [19] made a breakthrough by showing that these elusive ALPs may be detected when they convert into photons in the magnetic fields in 1983. This discovery presented a viable method for the detection of ALPs. Currently, many experiments are carried out searching for ALPs, of which the constraint given by the CERN Axion Solar Telescope (CAST) is $g_{a\gamma} < 6.6 \times 10^{-11}$ (GeV^{-1}) [14,20], with $g_{a\gamma}$ being the coupling of the ALP to diphoton. Still, more stringent bounds arise from astrophysical observations, of which the stellar evolution, determined using the R2 parameter, the ratio of stellar populations on the asymptotic giant branch to horizontal branch stars in globular clusters, gives $g_{a\gamma} < 4.7 \times 10^{-11}$ (GeV^{-1}) [21].

In addition to searching for ALPs with a Helioscope, there is currently a significant focus on utilizing DM direct detection experiments based on underground laboratories [22–25] to either directly detect ALPs or set novel constraints on ALP couplings in projected direct detection experiments. Either solar axions or heavy axion DM with large kinetic energy [26,27] can be detected in these experiments. Assuming that ALPs couple to neutrinos, the supernovae neutrinos can also boost the galactic DM ALPs via elastic scattering, resulting in relativistic ALPs [28]. In this paper, we will consider the direct detection signals of the ALP arising from the following three sources: (1) supernova neutrino-boosted ALPs ($v \sim c$); (2) solar axion; (3) galactic ALP DM($v \sim 10^{-3}c$) with large kinetic energy.

In this paper, we focus on the scattering process $a + e \to e + \gamma$, where a is an ALP, e and γ are electron and photon, respectively. This process, if mediated by the dimension-five operator $g_{a\gamma} a F_{\mu\nu} \tilde{F}_{\mu\nu}$, is called inverse Primakoff (IP) scattering [29,30]. Alternatively, the scattering mediated by the dimension-four operator $g_{ae} a \bar{e} i\gamma^5 e$ is called

[*]chaowei@bnu.edu.cn
[†]fengjj@mail.bnu.edu.cn
[‡]jinmj507@gmail.com

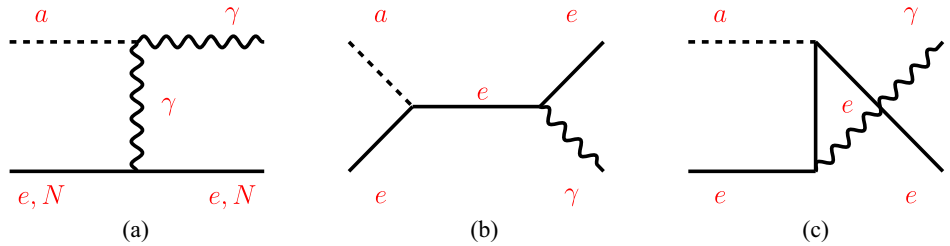

FIG. 1. Tree-level Feynman diagrams illustrating (a) the inverse Primakoff process and (b), (c) the inverse Compton process.

the inverse Compton (IC) scattering [31–33]. As shown in Figs. 1(a)–1(c), the coherent enhancement factor for the inverse Primakoff scattering is Z^2, with Z the atomic number of the target nucleus, which is similar to the Coulomb scattering process, while the coherent enhancement factor for the inverse Compton scattering is Z. Usually these two processes are separately considered in the literature by setting either $g_{a\gamma}$ or g_{ae} to be zero. However, the axion-photon and the axion-electron couplings may exist simultaneously in a real case, so one needs to account for the contribution to the scattering induced by the interference of two interactions, which is done in this paper. Our calculation shows that this contribution can be dominant for a large axion energy E_a, as can be seen in Fig. 2. The complete calculation helps to improve constraints on ALP couplings in projected DM direct detection experiments such as XENON, PandaX, etc.

Apart from the DM direct detection experiments mentioned above, an increasing number of researchers are interested in probing axions or ALPs using neutrino detectors, such as Super-K [34], JUNO [35], and others [36,37]. The strength of neutrino experiments lies in their substantial fiducial mass (∼20 kton), which helps to improve the exclusion limits. However, their drawback is that they can only search for ALPs with high energies due to the threshold of the detector. In this paper, we focus on the detectability of

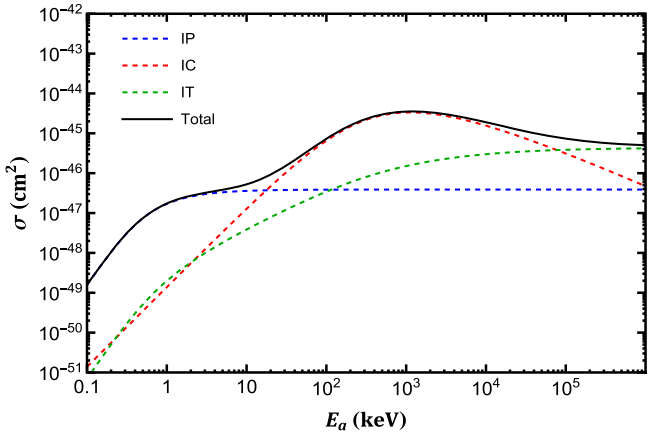

FIG. 2. The cross sections inverse Primakoff (blue dashed line), inverse Compton(red dashed line) and interference terms (green dashed line) conversion of ALP into photon. The black solid line represents the total cross section.

the supernova neutrino-boosted ALP, whose energy can reach MeV, using the JUNO detector. Projected constraints on ALP coupling at the 90% confidence level (C.L.) is presented in Fig. 7.

The remaining of the paper is organized as follows. In Sec. II, we calculate the scattering cross section $a + e \to e + \gamma$ induced the inverse Primakoff process, the inverse Compton process and the interference between these two terms. We discuss three fluxes of incoming axions; supernovae neutrino boosted ALPs, solar axions, and Galactic ALP DM in Sec. III. Then, we study the limitations of $g_{a\gamma}$ and g_{ae} in DM direct detection experiments. The constraints of JUNO are given in Sec. IV. Finally, summary remarks are given in the Sec. V.

II. ALP-ELECTRON SCATTERING

ALPs have gained attention in particle physics as they may play an important role in addressing various problems in terrestrial experiments and astrophysical observations, including DM and the strong CP problem. ALPs are assumed to be superlight and weakly interacting particles, and are predicted in certain extensions to the SM with spontaneous breaking global symmetries. Despite the possibility for ALPs to interact with a wide range of particles in various forms, most ALP models actually propose interactions specifically with photons and electrons with Lagrangian of the following form:

$$\mathcal{L} = -\frac{1}{4} g_{a\gamma} a F^{\mu\nu} \tilde{F}_{\mu\nu} + g_{ae} a \bar{e} i\gamma^5 e, \tag{1}$$

where a stands for the ALP. $F^{\mu\nu}$ is the electromagnetic field strength and its dual $\tilde{F}_{\mu\nu} = \frac{1}{2}\epsilon_{\mu\nu\alpha\beta}F^{\alpha\beta}$. $g_{a\gamma}$ and g_{ae} denote the axion-photon and axion-electron couplings, respectively. For the detection of ALPs, they can be probed via oscillations of ALP into the photon in a helioscope with constraint put on the coupling $g_{a\gamma}$. They can also be detected by the axioelectric effect by measuring the rate of atomic ionization induced by the absorption of ALP of the energies up to 100 keV [38]. Alternatively, they can be detected in direct detection experiments via the inverse Compton scattering [36,39,40] or the inverse Primakoff process [29,41–44] with the photon as the signal. In this paper, we focus on the photon signal of ALPs in

underground detectors, so we pay special attention to the inverse Compton scattering and the inverse Primakoff process, as well as their interference effect assuming g_{ae} and $g_{a\gamma}$ exist simultaneously.

Many experiments employ the inverse Primakoff scattering process of ALP with atoms as the detection channel, where the incoming ALPs are converted into photons in the electromagnetic field of the atom. It utilizes a screened Coulomb potential to portray the electrostatic field in the target atom. This potential takes the form of the Yukawa potential, with the screening length denoted as r_0. For the inverse Compton scattering process as shown in Figs. 1(b) and 1(c), the collision of ALP with the electron in the detector results in a photon in the final state. It should be mentioned that there is IP-like scattering process that also contribute to the $a + e \to e + \gamma$ scattering, as shown in Fig. 1(a), the interference of which with the traditional inverse Compton process has not been explicitly calculated.

The differential scattering cross section of the IP process is directly governed by the parameters $g_{a\gamma}$ and m_a, which determine the strength and characteristics of the interaction. The cross section of this process is obtained as

$$\frac{d\sigma^{\mathrm{IP}}}{d\Omega} = \frac{\alpha}{8\pi} g_{a\gamma}^2 \left[\frac{1}{(E_a + m_{e,N} - p_a \cos\theta)} \frac{E_\gamma^2}{p_a^3} \times (E_a - E_\gamma + 2m_{e,N}) \right] F_a^2(\boldsymbol{q}^2) \sin^2\theta, \tag{2}$$

where $\alpha = e^2/4\pi$ is the fine structure constant and $m_{e,N}$ is the electron or nucleus mass. For the incoming ALP of the mass m_a, its energy and momentum are E_a and $\boldsymbol{p_a}$, respectively, $p_a = |\boldsymbol{p_a}|$. The energy and momentum of the outgoing photon are E_γ and $\boldsymbol{p_\gamma}$. θ is the scattering angle and $\boldsymbol{q} = \boldsymbol{p_\gamma} - \boldsymbol{p_a}$ is the momentum transfer. An alternative method utilized in this paper to approximate the form factor $F_a(\boldsymbol{q}^2)$ involves assuming a screened Coulomb potential arising from the electrostatic field, resulting in $F_a(\boldsymbol{q}^2) = \frac{Zp_a^2}{\boldsymbol{q}^2 + r_0^{-2}}$ [41,42]. According to the energy conservation, one has

$$E_\gamma = \frac{2m_{e,N}E_a + m_a^2}{2(E_a + m_{e,N} - p_a \cos\theta)}. \tag{3}$$

Inserting Eq. (3) into Eq. (2) and then integrate over the solid angle, we can obtain $\sigma^{\mathrm{IP}}(g_{a\gamma}, E_a, m_a)$.

In the traditional calculation of the IP process, the nucleus recoil is neglected resulting in $E_\gamma \approx E_a$. Furthermore, if we ignore the mass of the ALP, the transfer momentum can be simplified as $|\boldsymbol{q}| = 2p_a \sin(\theta/2)$ and the factor $(E_a + m_{e,N} - p_a \cos\theta)$ can be approximated as $m_{e,N}$. In this approximation, our result in Eq. (2) can be simplified to the differential cross section which appear in most of the literature [29,41–44],

$$\frac{d\sigma_0^{\mathrm{IP}}}{d\Omega} = \frac{\alpha}{4\pi} g_{a\gamma}^2 F_a^2(\boldsymbol{q}^2) \sin^2\theta = \frac{\alpha}{16\pi} g_{a\gamma}^2 \frac{\boldsymbol{q}^2}{p_a^2} \left(4 - \frac{\boldsymbol{q}^2}{p_a^2}\right) F_a^2(\boldsymbol{q}^2). \tag{4}$$

The differential cross section for the inverse Compton scattering is given as [36,39,40]

$$\frac{d\sigma^{\mathrm{IC}}}{d\Omega} = \frac{Zg_{ae}^2}{8\pi m_e^2} \frac{\alpha E_\gamma}{p_a} \left(1 + \frac{4m_e^2 E_\gamma^2}{(2m_e E_a + m_a^2)^2} - \frac{4m_e E_\gamma}{(2m_e E_a + m_a^2)} - \frac{4m_a^2 p_a^2 m_e E_\gamma \sin^2\theta}{(2m_e E_a + m_a^2)^3}\right), \tag{5}$$

which is enhanced by the atomic number Z.

Most importantly, if there are axion-photon and axion-electron couplings simultaneously (i.e., both $g_{a\gamma}$ and g_{ae} are nonzero), the total squared matrix elements of the combined process exhibit interference between the traditional inverse Compton scattering terms given in Figs. 1(b) and 1(c) and the IP-like term given in Fig. 1(a). To assess the contributions of the interference terms, we define the cross section arising from the interference terms (IT) as σ^{IT}, which can be written as

$$\frac{d\sigma^{\mathrm{IT}}}{d\Omega} = \frac{\alpha}{8\pi} \frac{Zg_{a\gamma}g_{ae}E_\gamma^2}{(m_e + E_a - p_a\cos\theta)} \frac{p_a \sin^2\theta}{(\boldsymbol{q}^2 + r_0^{-2})} \times \left(\frac{1}{m_e + E_a - p_a\cos\theta} + \frac{1}{m_e}\right). \tag{6}$$

It should be mentioned that σ^{IT} is only enhanced by the factor Z, which is because we only account the interference of the inverse Compton scattering and the IP-like process induced by the Coulomb potential of the single electron.

Finally, the total cross section is $\sigma^{\mathrm{Tot}} = \sigma^{\mathrm{IP}} + \sigma^{\mathrm{IC}} + \sigma^{\mathrm{IT}}$. We explore the contribution of each term, as depicted in Fig. 2, varies with ALP energy (E_a). The depicted figure represents a scenario with parameters set as $g_{a\gamma} = 10^{-10}$ (GeV^{-1}), $g_{ae} = 10^{-11}$, $Z = 54$ (Xe), $r_0 = 2.45$ Å (LXe), $m_a = 10^{-9}$ keV. If we alter the coupling constants as well as the target material, the contributions of each process will undergo changes.

In addition, ALP can decay into diphoton with the decay width [6,36,45]

$$\Gamma = \frac{g_{a\gamma}^2 m_a^3}{64\pi}. \tag{7}$$

The lifetime of ALP is then given as $\tau_a = \Gamma^{-1}$. When the ALP mass (or $g_{a\gamma}$) is small enough, its lifetime can be longer than the age of the universe. Alternatively, there is constraint on the mass of ALP and its coupling $g_{a\gamma}$ from the stability of ALP. In the following analysis, we assume that $g_{a\gamma}$ is small enough so as to avoid the stability constraint for

Galactic ALP DM ($v \sim 10^{-3}c$), which has $g_{a\gamma} < 5.4 \times 10^{-16}$ (GeV^{-1}) for $m_a = 1000$ keV.

III. DIRECT DETECTION SIGNAL

In this section, we discuss the photon signal of ALP in DM direct detection experiments by accounting the contribution of the interference given in the last section. We will first discuss the ALP flux used in the calculation, then we show constraints of current and projected direct detection experiments on ALP couplings.

A. ALP flux

1. Neutrino-boosted ALP flux

The possibility of boosting ALPs by elastic scattering of supernova neutrinos with ALPs is discussed in Refs, [28,46]. Consequently, the ALP energy experiences a substantial amplification, leading them to exhibit characteristics of relativistic particles. Although the scattering cross section is small, the huge neutrino flux greatly enhances the ALP flux, which helps to increase the number event of the direct detection. We conservatively estimate the ALP flux by ignoring the effect of neutrino oscillations, and the boosted ALP flux given in the Ref. [28] is applied in our analysis.

2. Solar axion flux

Both axion-photon and axion-electron couplings are important parameters to determine the solar axion flux. The axion-electron coupling induces a large number of reactions that are significant. The most important processes are the ABC reactions; Atomic axiorecombination [47,48] and atomic axiodeexcitation, axio-Bremsstrahlung in electron-ion [49,50] or electron-electron collisions, and Compton scattering [51–53]. In fact, there is uncertainty in the ABC processes. Sebastian Hoof *et al.* [54] have analyzed this problem and the results are very similar to these from Redondo [17], so we only refer to the solar axion flux given by Redondo [17] in this paper. The axion flux, arising from the Primakoff effect [55,56], cannot be neglected in certain cases. We use the formula [57–59],

$$\frac{d\Phi_a}{dE_a} = 6 \times 10^{10} \left(\frac{g_{a\gamma}}{10^{-10}\ \mathrm{GeV}^{-1}} \right)^2 \times \left(\frac{E_a}{\mathrm{keV}} \right)^{2.481} \exp^{-E_a/(1.205\ \mathrm{keV})}\ \mathrm{cm}^{-2}\,\mathrm{s}^{-1}\,\mathrm{keV}^{-1} \quad (8)$$

to calculate the axion flux from the Primakoff effect.

In this paper, the ALP flux comprises both the ABC process and the Primakoff process. We reference the solar axion flux reported in Ref. [17] (for details regarding the solar axion flux, see Ref. [17,18,60]).

3. ALP DM flux

If we assume that ALPs exclusively make up the entirety of the galactic DM density, the total flux of ALP DM is

$$\Phi_a = \frac{\rho_{\mathrm{DM}}}{m_a} v_a. \quad (9)$$

Where m_a, v_a, and ρ_a are the mass, velocity and the local energy density of the ALP, respectively. Precisely, the local DM density in the solar system is taken as $\rho_{\mathrm{DM}} = (0.2\text{–}0.6)\ \mathrm{GeV/cm}^3$ [61,62]. The flux of ALP DM can be expressed by

$$\Phi_a = \frac{1\ \mathrm{keV}}{m_a} \times 9 \times 10^{12}\ (\mathrm{cm}^{-2} \cdot \mathrm{s}^{-1}), \quad (10)$$

by taking $\rho_{\mathrm{DM}} = 0.3\ \mathrm{GeV/cm}^3$ [26,63] and $v_a \sim 10^{-3}c$. If one accounts for the effect of the DM local velocity, Eq. (10) should be multiplied by the factor of the Maxwell-Boltzmann distribution [64].

We show the flux of the solar axion and neutrino boosted ALP in Fig. 3, in which the blue and orange curves represent the flux induced by the ABC processes and the Primakoff process, respectively. The green curve represents the neutrino boosted ALP flux enhanced by the factor of 10^5. For the ALP DM flux, we use the Eq. (10) directly.

B. Direct detection constraints

In this subsection, we study signals for three types of ALP fluxes in DM direct detection experiments so as to put constraints on ALP couplings. The expected number of events for signals due to the inverse Primakoff, inverse

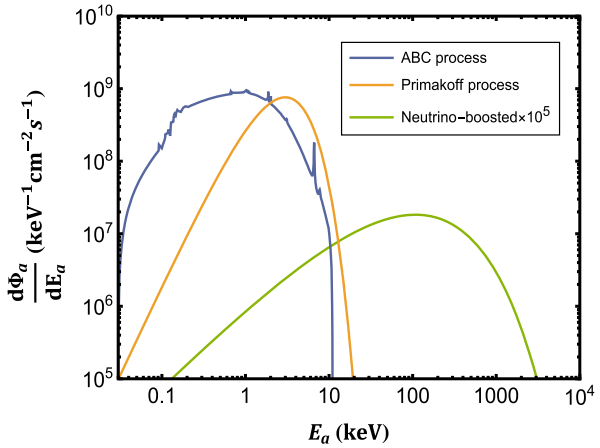

FIG. 3. The blue line represents the solar axion flux produced by the ABC processes with $g_{ae} = 10^{-13}$ [17]. The orange line represents the solar axion flux generated by the Primakoff process with $g_{a\gamma} = 10^{-11}$ (GeV^{-1}) [57–59]. Neutrino-boosted ALP flux is shown as green line with $m_a = 10^{-15}$ keV [28]. Note that the green line has been scaled up by a factor 10^5 to make it visible.

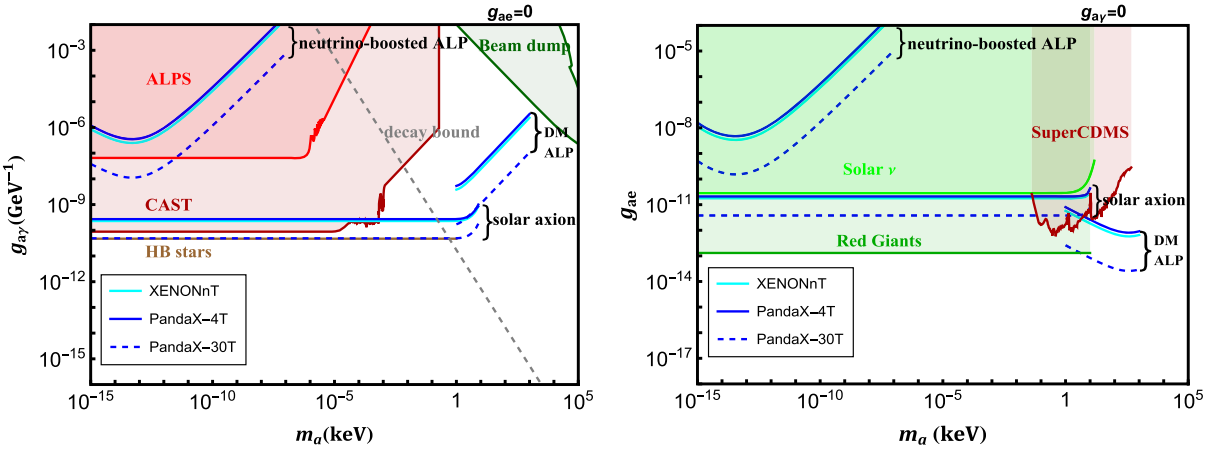

FIG. 4. 90% C.L. limits on axion-photon (axion-electron) coupling $g_{a\gamma}(g_{ae})$ versus ALP mass in the left (right) panel. The blue solid, cyan solid, and blue dashed lines represent constraints of direct detection experiments PandaX-4T, XENONnT, and PandaX-30T, respectively, applied to three different incoming ALP fluxes; neutrino-boosted ALP, solar axion, and Galactic ALP DM. For comparison, other search experiments including ALPS (red) [69], CAST (darker red) [14,20], Beam dump (green) [70–74] and horizontal branch stars (brown) [21] are also shown in left panel. And there is stability constraint as ALP can decay into photons(gray dashed line). In right panel, the bounds from solar neutrino flux (green) [75] and red giants (darker green) [76], underground detectors SuperCDMS (darker red) [77] are added.

Compton, and their interference in the detector is given by [35,65]

$$N_{\text{event}} = N_T \cdot \Phi_a \cdot (\sigma^{\text{IP}} + \sigma^{\text{IC}} + \sigma^{\text{IT}}) \cdot \epsilon, \qquad (11)$$

where N_T is the number of targets and Φ_a denote the flux of the incoming ALP, with the subindex a denoting three distinct types of fluxes described in Sec. III A, and ϵ represents the detector efficiency. In the following, we assume $\epsilon = 1$ for all detection channels.

We can define the signal-to-noise ratio of the signal as the quantity $r_{\text{sn}} = \frac{S}{\sqrt{N_{\text{bkg}}+S}}$. N_{bkg} is the total number of background events. The value of S is determined using the Feldman-Cousins 90% upper confidence level of signal events, with $r_{\text{sn}} \sim 1.64$ [46]. Thus by comparing the S to N_{event} times the detector target exposure $T \times W$, where T and W are the exposure time and the weight of the target, respectively, we can derive the 90% C.L. limits on g_{ae} and $g_{a\gamma}$. For (projected) DM direct detection experiments XENONnT, PandaX-4T, and PandaX-30T, the exposure are taken as 1.16, 0.63, and 30 ton-years, respectively [16,66–68].

We first assume $g_{ae} = 0$ and $g_{a\gamma} \neq 0$, such that the number of expected events is simplified to $N_{\text{event}} = N_T \cdot \Phi_a \cdot \sigma^{\text{IP}}$. The resulting 90% C.L. limits are given in the left panel of Fig. 4, which shows $g_{a\gamma}$ versus m_a for various experiments. The blue solid, cyan solid, and blue dashed lines represent the constraints of direct detection experiments PandaX-4T, XENONnT, and PandaX-30T, respectively. For comparison, the bounds from the ALPS (red) [69], CAST (darker red) [14,20], beam dump (green) [70–74] and horizontal branch stars (brown) [21] are also added. Constraints on the neutrino-boosted ALPs are shown in the top-left corner of the figure. The contribution of the ABC processes to the solar ALP flux is removed when $g_{ae} = 0$, thus we only consider the ALP flux generated by the Primakoff effect, which is proportional to $g_{a\gamma}^2$. Its constraints are shown as horizontal lines at the center of the figure. The stability constraint on m_a and $g_{a\gamma}$ is added to the plot in the left-panel of Fig. 4, marked as gray dashed line, to the right part of which $\tau_a < 13.8$ billion years. The direct detection constraints with ALP flux arising from the galactic DM are shown in Fig. 4, where the detector threshold for the xenon target considered here is about $\mathcal{O}(1)$ keV [16,22]. Though these constraints do not reach the limits set by astrophysical observations, they can be improved in the future by increasing the exposure or advancing the detection technology.

For the case $g_{a\gamma} = 0$ and $g_{ae} \neq 0$, the number of events is given as $N_{\text{event}} = N_T \cdot \Phi_a \cdot \sigma^{\text{IC}}$. The 90% C.L. limits of g_{ae} are shown in the right panel of Fig. 4. Other limits include solar neutrino flux (green) [75], red giants (darker green) [76,78] and underground detectors SuperCDMS (darker red) [77]. The analysis is similar to the previous case except that the source of the solar axion flux is induced by the ABC processes. For ALP DM, σ^{IC} increases with m_a when $m_a < 1$ MeV, so the upper limit on g_{ae} is inversely proportional to m_a. We restrict ALP mass to 1 MeV to avoid it decaying into electron-positron pair.

For the case $g_{a\gamma} \neq 0$ and $g_{ae} \neq 0$, we use Eq. (11) directly to constrain the two couplings. We show the upper limits on $g_{a\gamma}$ by fixing $g_{ae} = 10^{-14}$ in the left panel of Fig. 5, and find more stringent constraints put by the solar ALP flux. Since both g_{ae} and $g_{a\gamma}$ are nonzero, the solar ALP flux is

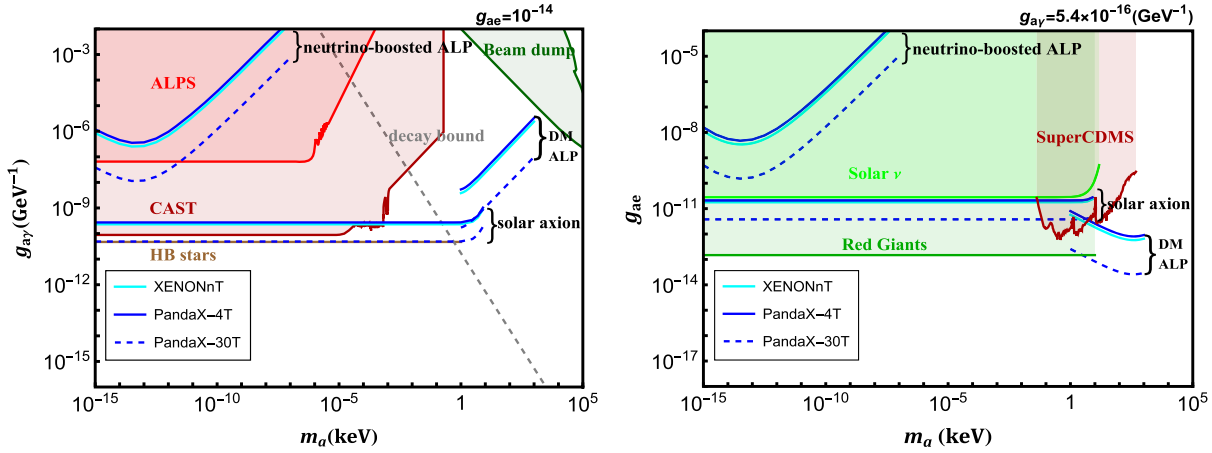

FIG. 5. 90% C.L. limits on axion-photon or axion-electron coupling constants versus ALP mass. We set $g_{ae} = 10^{-14}$ and $g_{a\gamma} = 5.4 \times 10^{-16}$ (GeV^{-1}) in left and right panel, respectively. The gray dashed line indicates the stability constraint.

attributed to ABC and Primakoff processes. We further see that the limits of pandaX-30T in the future is almost comparable to the limits from astronomical observations, which is a very promising trend. Alternatively, we show the exclusion limits on the g_{ae} in the right panel of Fig. 5. Since $g_{a\gamma}$ is very small in this case, the solar ALP flux generated by Primakoff effect is almost negligible compared to the ABC processes. We set $g_{a\gamma} = 5.4 \times 10^{-16}$ GeV^{-1} in the right panel of Fig. 5, which guarantees that the ALP is stable with mass up to 1000 keV.

Furthermore, we have scanned two parameters $g_{a\gamma}$ and g_{ae}. In Fig. 6, we show the resulting 90% C.L. constraints on the $g_{ae} - g_{a\gamma}$ plane given by the XENONnT and PandaX-30T. Since the constraint of the pandaX-4T is very similar to that of the XENONnT, we only show the results of XENONnT for simplification. In small-mass case, $m_a = 10^{-4}$ keV, the incoming ALP flux is mainly from the solar ALPs. The gray lines are exclusion limits from astrophysical observations. We find that there is still parameter space that survives in astrophysical bounds but can be excluded by future projected direct detection experiments, providing added confidence for further investigations.

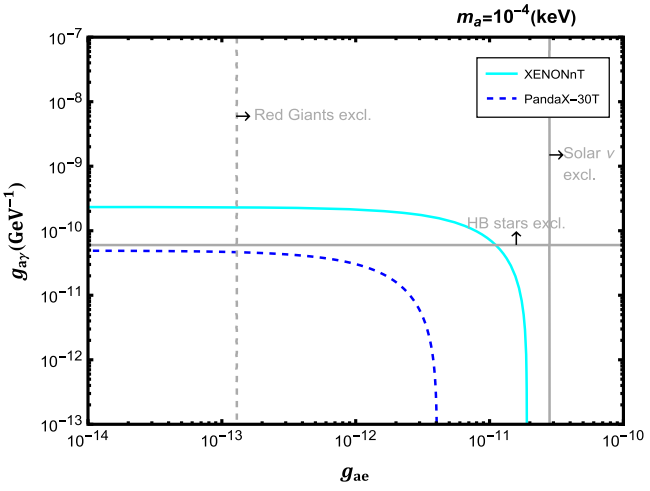

FIG. 6. 90% C.L. limits on g_{ae}–$g_{a\gamma}$ plane in XENONnT and PandaX-30T. Gray lines represent the constraints from astrophysical bounds including red giants [78] and the horizontal branch stars [21], as well as the constraints from the solar neutrino [75], with arrows denoting excluded regions. We take $m_a = 10^{-4}$ keV in the figure.

IV. JUNO CONSTRAINTS

The next-generation multipurpose Jiangmen Underground Neutrino Observatory (JUNO) [79–83] is a state-of-the-art neutrino experiment primarily designed to investigate the properties of neutrinos, but it also has the potential to contribute to the search for new physics beyond the Standard Model, such as proton decay [79], hidden sector particles [84], and axions [35], etc. In this paper, we employ the JUNO detection experiment to set boundaries on the couplings of ALP. Thanks to its extensive exposure, we can significantly restrict the allowable values of the couplings.

One of the main components of the JUNO is the central detector, which is a massive, spherical acrylic sphere filled with a high-purity liquid scintillator (LS). The detection medium is a linear alkylbenzene (LAB) composed of 19 carbon atoms $C_{19}H_{32}$, which has excellent transparency, high flash point, low chemical reactivity, and good light yield. The LS is also doped with 3 g/L of 2,5-diphenyloxazole (PPO) and 15 mg/L of pbis-(o-methylstyryl)-benzene (bis-MSB). The density of the LS is 0.859 g/ml, with a total of 20 ktons in a spherical container with a radius of 17.7 meters. The central detector is submerged in a cylindrical pool to protect it from the radioactivity of the surrounding rock. On the top of the water pool, a muon tracker will be installed. We refer the reader to Ref. [79] for more details about the JUNO.

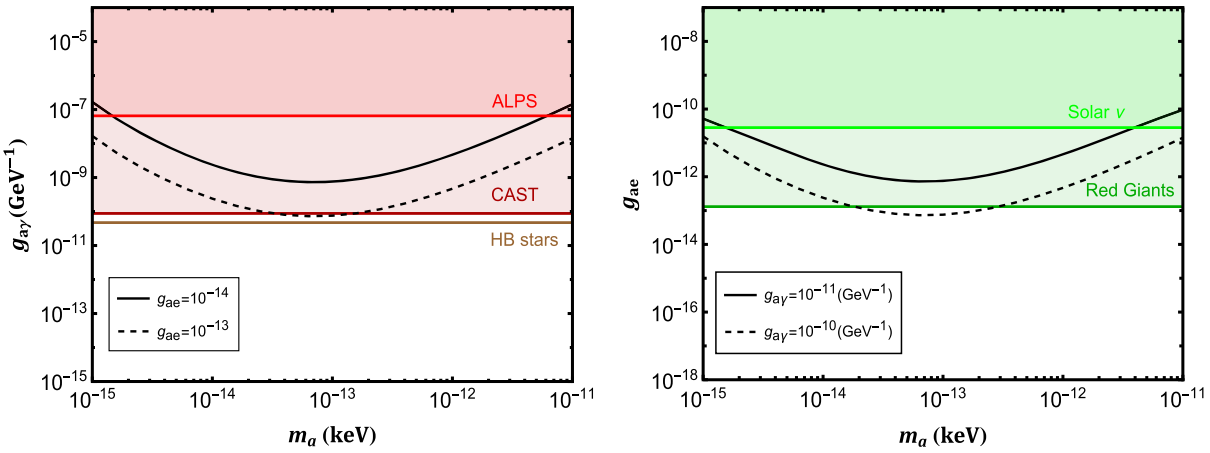

FIG. 7. 90% C.L. limits on $g_{a\gamma}(g_{ae})$–m_a planes in JUNO. Left panel: Black solid (dashed) line represent $g_{ae} = 10^{-14}$ (10^{-13}). Right panel: Black solid (dashed) line represents $g_{a\gamma} = 10^{-11}$ (10^{-10}) GeV^{-1}.

Due to the threshold of the detector ($E_{\rm th} \geq 0.8$ MeV), both the solar ALPs and the ALP DM fluxes are almost undetectable in the JUNO, leaving the supernova neutrino-boosted ALP as the only possible way out. The ALP fluxes have been discussed in Sec. III.A. Similar to the discussion in the Sec. III.B, we still use $\sigma^{\rm Tot} = (\sigma^{\rm IP} + \sigma^{\rm IC} + \sigma^{\rm IT})$ to constrain limits. The expected number of events per unit time is

$$N_{\rm event} = N_e \cdot \Phi_a \cdot (\sigma^{\rm IP} + \sigma^{\rm IC} + \sigma^{\rm IT}) \cdot \mathcal{R} \cdot \epsilon, \quad (12)$$

where $N_e \simeq 5.5 \times 10^{33}$ is the number of electrons in the 16.2 kton fiducial volume. $\mathcal{R}$ and ϵ represent the detector energy resolution and efficiency, respectively. The following discussion assumes that $\epsilon = 1$ and over the energy threshold. Here, we use the likelihood function in Ref. [83] to conduct numerical analysis. Reference [84] shows the total number of events (S) expected to be detected over a ten year period, $S = 97$, corresponding to a 90% C.L. sensitivity. Therefore, we use $S_{\rm limit} = 97$ counts for ten years of data. The number of events used to constrain the upper limit on ALP couplings satisfy $S = N_{\rm event} \cdot T \leq S_{\rm limit}$, and $T = 10$ years. In this way, the numerical results are shown in Fig. 7.

We choose to forecast the sensitivity at the 90% C.L. to make a direct comparison with constraints of DM direct detection experiments. Our result shows that the exclusion limits of the JUNO experiment are enhanced by approximately two orders of magnitude compared to direct detection experiments, owing to the substantial fiducial volume of JUNO. It is worth noting that even in the case of the next-generation PandaX-30T experiment, JUNO is likely to provide constraints on ALP couplings that are approximately one order of magnitude tighter. The most stringent constraints on couplings have been reached $g_{a\gamma} < 7 \times 10^{-10}$ (GeV^{-1}) and $g_{ae} < 7.5 \times 10^{-13}$, which are better than constraints from astrophysical bounds. It should be mentioned that these are very conservative limits, as we have considered small values for both g_{ae} (left panel) and $g_{a\gamma}$ (right panel) in Fig. 7.

V. CONCLUSION

The direct detection of ALPs is an important issue as the ALP itself serves a promising DM candidate and may solve the strong CP problem. In addition to cavity experiments, which measure $g_{a\gamma}$ via oscillations of ALP into photon in electromagnetic fields, direct detection experiments may also detect ALP via the inverse Compton process or inverse Primakoff process. In this paper, we pay special attention to the calculation of the process $a + e \to e + \gamma$, and show the interference between the inverse Primakoff and inverse Compton amplitudes. We have shown constraints of projected direct detection experiments on couplings g_{ae} and $g_{a\gamma}$. We further studied the constraints of the JUNO Cherenkov detector on these couplings. This study provides theoretical support for the detections of ALPs.

ACKNOWLEDGMENTS

This work was supported by the National Natural Science Foundation of China (NSFC) (Grants No. 11775025 and No. 12175027).

[1] R. D. Peccei and H. R. Quinn, Phys. Rev. Lett. **38**, 1440 (1977).
[2] R. D. Peccei and H. R. Quinn, Phys. Rev. D **16**, 1791 (1977).
[3] S. Weinberg, Phys. Rev. Lett. **40**, 223 (1978).
[4] F. Wilczek, Phys. Rev. Lett. **40**, 279 (1978).
[5] Z. G. Berezhiani and M. Y. Khlopov, Z. Phys. C **49**, 73 (1991).
[6] J. Preskill, M. B. Wise, and F. Wilczek, Phys. Lett. **120B**, 127 (1983).
[7] L. F. Abbott and P. Sikivie, Phys. Lett. **120B**, 133 (1983).
[8] M. Dine and W. Fischler, Phys. Lett. **120B**, 137 (1983).
[9] J. E. Kim and G. Carosi, Rev. Mod. Phys. **82**, 557 (2010); **91**, 049902(E) (2019).
[10] J. L. Feng, Annu. Rev. Astron. Astrophys. **48**, 495 (2010).
[11] H. Tam and Q. Yang, arXiv:1108.3362.
[12] D. J. E. Marsh, Phys. Rep. **643**, 1 (2016).
[13] A. Spector (ALPS Collaboration), in *14th Patras Workshop on Axions, WIMPs and WISPs* (2019), arXiv:1906.09011.
[14] V. Anastassopoulos *et al.* (CAST Collaboration), Nat. Phys. **13**, 584 (2017).
[15] D. S. Akerib *et al.* (LUX Collaboration), Phys. Rev. Lett. **118**, 261301 (2017).
[16] E. Aprile *et al.* (XENON Collaboration), Phys. Rev. Lett. **129**, 161805 (2022).
[17] J. Redondo, J. Cosmol. Astropart. Phys. 12 (2013) 008.
[18] A. V. Derbin, I. S. Drachnev, A. S. Kayunov, and V. N. Muratova, JETP Lett. **95**, 339 (2012).
[19] P. Sikivie, Phys. Rev. Lett. **51**, 1415 (1983); **52**, 695(E) (1984).
[20] S. Andriamonje *et al.* (CAST Collaboration), J. Cosmol. Astropart. Phys. 04 (2007) 010.
[21] M. J. Dolan, F. J. Hiskens, and R. R. Volkas, J. Cosmol. Astropart. Phys. 10 (2022) 096.
[22] C. Fu *et al.* (PandaX Collaboration), Phys. Rev. Lett. **119**, 181806 (2017).
[23] S. Knapen, T. Lin, H. K. Lou, and T. Melia, Phys. Rev. Lett. **118**, 171801 (2017).
[24] G. Aad *et al.* (ATLAS Collaboration), J. High Energy Phys. 03 (2021) 243; 11 (2021) 50.
[25] P. Agnes *et al.* (DarkSide Collaboration), Phys. Rev. Lett. **130**, 101002 (2023).
[26] K. Arisaka, P. Beltrame, C. Ghag, J. Kaidi, K. Lung, A. Lyashenko, R. D. Peccei, P. Smith, and K. Ye, Astropart. Phys. **44**, 59 (2013).
[27] I. G. Irastorza and J. Redondo, Prog. Part. Nucl. Phys. **102**, 89 (2018).
[28] P. Carenza and P. De la Torre Luque, Eur. Phys. J. C **83**, 110 (2023).
[29] W. Buchmuller and F. Hoogeveen, Phys. Lett. B **237**, 278 (1990).
[30] R. J. Creswick, F. T. Avignone, III, H. A. Farach, J. I. Collar, A. O. Gattone, S. Nussinov, and K. Zioutas, Phys. Lett. B **427**, 235 (1998).
[31] F. T. Avignone, C. Baktash, W. C. Barker, F. P. Calaprice, R. W. Dunford, W. C. Haxton, D. Kahana, R. T. Kouzes, H. S. Miley, and D. M. Moltz, Phys. Rev. D **37**, 618 (1988).
[32] R. Chanda, J. F. Nieves, and P. B. Pal, Phys. Rev. D **37**, 2714 (1988).
[33] S. J. Brodsky, E. Mottola, I. J. Muzinich, and M. Soldate, Phys. Rev. Lett. **56**, 1763 (1986); **57**, 502(E) (1986).
[34] T. Li and R.-J. Zhang, Phys. Rev. D **106**, 095034 (2022).
[35] G. Lucente, N. Nath, F. Capozzi, M. Giannotti, and A. Mirizzi, Phys. Rev. D **106**, 123007 (2022).
[36] J. B. Dent, B. Dutta, D. Kim, S. Liao, R. Mahapatra, K. Sinha, and A. Thompson, Phys. Rev. Lett. **124**, 211804 (2020).
[37] A. Bhusal, N. Houston, and T. Li, Phys. Rev. Lett. **126**, 091601 (2021).
[38] A. Derevianko, V. A. Dzuba, V. V. Flambaum, and M. Pospelov, Phys. Rev. D **82**, 065006 (2010).
[39] T. W. Donnelly, S. J. Freedman, R. S. Lytel, R. D. Peccei, and M. Schwartz, Phys. Rev. D **18**, 1607 (1978).
[40] G. Bellini *et al.* (Borexino Collaboration), Eur. Phys. J. C **54**, 61 (2008).
[41] F. T. Avignone, III *et al.* (SOLAX Collaboration), Phys. Rev. Lett. **81**, 5068 (1998).
[42] T. Abe, K. Hamaguchi, and N. Nagata, Phys. Lett. B **815**, 136174 (2021).
[43] J. B. Dent, B. Dutta, J. L. Newstead, and A. Thompson, Phys. Rev. Lett. **125**, 131805 (2020).
[44] C. Gao, J. Liu, L.-T. Wang, X.-P. Wang, W. Xue, and Y.-M. Zhong, Phys. Rev. Lett. **125**, 131806 (2020).
[45] E. Charles *et al.* (Fermi-LAT Collaboration), Phys. Rep. **636**, 1 (2016).
[46] Y.-H. Lin, W.-H. Wu, M.-R. Wu, and H. T.-K. Wong, Phys. Rev. Lett. **130**, 111002 (2023).
[47] S. Dimopoulos, G. D. Starkman, and B. W. Lynn, Mod. Phys. Lett. A **1**, 491 (1986).
[48] M. Pospelov, A. Ritz, and M. B. Voloshin, Phys. Rev. D **78**, 115012 (2008).
[49] A. R. Zhitnitsky and Y. I. Skovpen, Sov. J. Nucl. Phys. **29**, 513 (1979).
[50] L. M. Krauss, J. E. Moody, and F. Wilczek, Phys. Lett. **144B**, 391 (1984).
[51] K. O. Mikaelian, Phys. Rev. D **18**, 3605 (1978).
[52] M. Fukugita, S. Watamura, and M. Yoshimura, Phys. Rev. Lett. **48**, 1522 (1982).
[53] M. Fukugita, S. Watamura, and M. Yoshimura, Phys. Rev. D **26**, 1840 (1982).
[54] S. Hoof, J. Jaeckel, and L. J. Thormaehlen, J. Cosmol. Astropart. Phys. 09 (2021) 006.
[55] G. G. Raffelt, Phys. Rev. D **33**, 897 (1986).
[56] G. G. Raffelt, Phys. Rev. D **37**, 1356 (1988).
[57] C. Hagmann, H. Murayama, G. G. Raffelt, L. J. Rosenberg, and K. v. Bibber (2008).
[58] Z. Ahmed *et al.* (CDMS Collaboration), Phys. Rev. Lett. **103**, 141802 (2009).
[59] E. Arik *et al.* (CAST Collaboration), J. Cosmol. Astropart. Phys. 02 (2009) 008.
[60] M. Asplund, N. Grevesse, A. J. Sauval, and P. Scott, Annu. Rev. Astron. Astrophys. **47**, 481 (2009).
[61] N. Aghanim *et al.* (Planck Collaboration), Astron. Astrophys. **641**, A6 (2020); **652**, C4(E) (2021).
[62] R. L. Workman *et al.* (Particle Data Group), Prog. Theor. Exp. Phys. **2022**, 083C01 (2022).
[63] A. Branca *et al.*, Phys. Rev. Lett. **118**, 021302 (2017).
[64] M. Lisanti, in *New Frontiers in Fields and Strings* (World Scientific, Singapore, 2017), pp. 399–446.

[65] J. D. Vergados, P. C. Divari, and H. Ejiri, Adv. High Energy Phys. **2022**, 7373365 (2022).
[66] Y. Meng *et al.* (PandaX-4T Collaboration), Phys. Rev. Lett. **127**, 261802 (2021).
[67] X. Wang, Z. Lei, Y. Ju, J. Liu, N. Zhou, Y. Chen, Z. Wang, X. Cui, Y. Meng, and L. Zhao, J. Instrum. **18**, P05028 (2023).
[68] J. Liu, X. Chen, and X. Ji, Nat. Phys. **13**, 212 (2017).
[69] K. Ehret *et al.*, Phys. Lett. B **689**, 149 (2010).
[70] F. Bergsma *et al.* (CHARM Collaboration), Phys. Lett. **157B**, 458 (1985).
[71] E. M. Riordan *et al.*, Phys. Rev. Lett. **59**, 755 (1987).
[72] M. J. Dolan, T. Ferber, C. Hearty, F. Kahlhoefer, and K. Schmidt-Hoberg, J. High Energy Phys. 12 (2017) 094; 03 (2021) 190.
[73] J. Blumlein *et al.*, Z. Phys. C **51**, 341 (1991).
[74] D. Banerjee *et al.* (NA64 Collaboration), Phys. Rev. Lett. **125**, 081801 (2020).
[75] P. Gondolo and G. G. Raffelt, Phys. Rev. D **79**, 107301 (2009).
[76] O. Straniero, C. Pallanca, E. Dalessandro, I. Dominguez, F. R. Ferraro, M. Giannotti, A. Mirizzi, and L. Piersanti, Astron. Astrophys. **644**, A166 (2020).
[77] T. Aralis *et al.* (SuperCDMS Collaboration), Phys. Rev. D **101**, 052008 (2020); **103**, 039901(E) (2021).
[78] F. Capozzi and G. Raffelt, Phys. Rev. D **102**, 083007 (2020).
[79] F. An *et al.* (JUNO Collaboration), J. Phys. G **43**, 030401 (2016).
[80] Z. Djurcic *et al.*, arXiv:1508.07166.
[81] A. Abusleme *et al.* (JUNO Collaboration), Chin. Phys. C **45**, 023004 (2021).
[82] A. Abusleme *et al.* (JUNO Collaboration), J. High Energy Phys. 03 (2021) 004.
[83] A. Abusleme *et al.* (JUNO Collaboration), Prog. Part. Nucl. Phys. **123**, 103927 (2022).
[84] F. D'Eramo, G. Lucente, N. Nath, and S. Yun, J. High Energy Phys. 12 (2023) 091.